Multi-Sensor Scene Modeling Using Statistical Models for Bidirectional Texture Functions

[1]Peter Bajcsy, [1]Rob Kooper and [2]Dennis Andersh
[1]National Center for Supercomputing Applications (NCSA)
University of Illinois at Urbana-Champaign, IL
and
[2] Scientific Applications International Corporation (SAIC), Champaign, IL
Email: pbajcsy@ncsa.uiuc.edu, kooper@ncsa.uiuc.edu, dennis.j.andersh@SAIC.COM

ABSTRACT

This paper presents a novel approach to multi-sensor statistical modeling of bi-directional texture functions (BTF). Our proposed BTF modeling approach is based on (1) conducting an analytical study that relates a sensor resolution to the size and shape of elements forming material surface, (2) developing a robotic system for laboratory BTF data acquisition, (3) researching an application of the Johnson family of statistical probability distribution functions (PDF) to BTF modeling, (4) selecting optimal feature space for statistical BTF modeling, (5) building a database of parameters for the Johnson family of PDFs that after interpolations forms a high-dimensional statistical BTF model and (6) researching several statistical quality metrics that can be used for verification and validation of the obtained BTF models. The motivation for developing the proposed statistical BTF modeling approach comes from the facts that (a) analytical models have to incorporate randomness of outdoor scene clutter surfaces and (b) models have to be computationally feasible with respect to the complexity of modeled interactions between light and materials. The major advantages of our approach over other approaches are (a) the low computational requirements on BTF modeling (BTF model storage, fast BTF model-based generation), (b) flexibility of the Johnson family of PDFs to cover a wide range of PDF shapes and (c) applicability of the BTF model to a wide range of spectral sensors, e.g., color, multi-spectral or hyperspectral cameras. The prime applications for the proposed BTF model are multi-sensor automatic target recognition (ATR), and scene understanding and simulation.

Keywords: Bidirectional reflectance distribution functions, statistical modeling.

1. INTRODUCTION

Physics-based surface appearance modeling is based on developing models for bi-directional reflectance distribution functions (BRDF) at coarse scale and bi-directional texture functions (BTF) at fine scale for a range of incident and viewing angles (see Figure 1). The scale is usually defined as a ratio of the sensor (camera) spatial resolution and a roughness variation of the corresponding constant-color imaged surface. BTF are known to depend on incident illumination angles, viewing angles, incident wavelengths and the interaction of light with each material patch (surface and body properties) that contributes to one value measured by a sensor, for example, one pixel value of a camera sensor. In general, the goal of BTF modeling is to predict a spatial distribution of pixel values given incident illumination angles, viewing angles, wavelength and the viewed material description assuming that (a) a BTF model is sensor and light propagation media invariant or (b) a BTF model compensates for any changes due to sensor and light propagation media characteristics. Specifically, we focus on those multi-sensor BTF representations that correspond to sensors operating at either different wavelengths, such as, thermal infrared (IR) and color visible spectrum cameras, or the same wavelengths but based on different data acquisition mechanism, for instance, hyperspectral and color visible spectrum cameras.
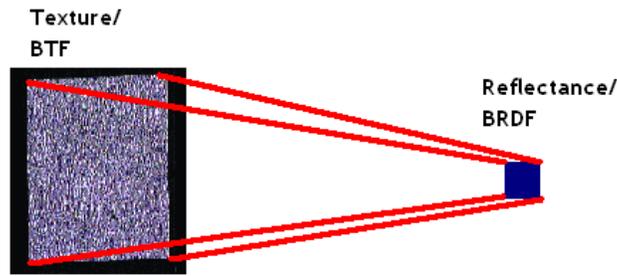
Figure 1: Fine scale texture model using BTF (left) and coarse scale reflectance model using BRDF (right).

BTF have been used in computer vision for object recognition (texture models), robotics (photometric stereo and depth from shading algorithms for depth information recovery) and in computer graphics for virtual world rendering, training and simulations. There are also ubiquitous applications of BTF in the areas of (a) geographic information systems (GIS), e.g., satellite image analysis to obtain land use maps, (b) military, e.g., to simulate battlefield scenarios, or (c) space exploration, e.g., navigation of space rowers.

The complexity of BTF cannot be easily modeled with analytical models due to the randomness of outdoor scene surfaces (geometrical surface randomness) or due to difficulties in deriving analytical models for real materials (complex interaction of light with materials). For example, it is very hard to model every blade of grass with accurate 3D geometry. Similarly, it is hard to model materials with wavelength dependencies, e.g., wavelength dependent absorbent surfaces and fluorescing materials, or the light and material interactions with quantum light behavior, e.g., energy saturation and saturation of kinetic energy. Furthermore, any outdoor BTF modeling requires considering (a) temporally changing spectral properties of the solar illumination, (b) all atmospheric effects on the solar illumination and (c) seasonal vegetation changes. Any BTF model has to incorporate various types of input information as it is illustrated in Figure 2. These types of input information and their associated uncertainty can significantly impact the accuracy of BTF models regardless of the underlying prediction model accuracy. For instance, running a very accurate simulation model with inaccurate (or highly uncertain) input parameters will lead to inaccurate predictions. In addition, from the BTF model building view point, very complex analytical models usually require large computational resources that might make the models impractical for a use in real applications, such as, multi-sensor automatic target recognition (ATR) and scene understanding. Thus, the aforementioned challenges in BTF modeling motivated our work on developing statistical BTF models that are closely related to the analytical models derived from Maxwell equations and geometrical optics, but computationally inexpensive and therefore more suitable for practical use in the area of multi-sensor ATR and scene modeling.

Our BTF modeling approach is based on (1) conducting an analytical study that relates a sensor resolution (e.g., physical area captured by one image pixel) to the size and shape of elements forming material surface (e.g., grains of sand), (2) developing a robotic system for laboratory BTF data acquisition, (3) researching an application of the Johnson family of statistical probability distribution functions (PDF) to BTF modeling, (4) selecting optimal feature space for statistical BTF modeling, (5) building a database of PDF parameters for the Johnson family of PDFs that after interpolations forms a high-dimensional statistical BTF model and (6) researching several statistical quality metrics that can be used for verification and validation of the obtained BTF models. Although our BTF modeling approach is based on extracting statistical parameters from measured data and generating synthetic data based on the extracted information in a database, we are working on relating the proposed statistical model to the analytical models as it has been performed for the BRDF models of Nayar (Columbia University) and Koenderink (Utrecht, NL) [5] and BTF models of Dana and Nayar [6].
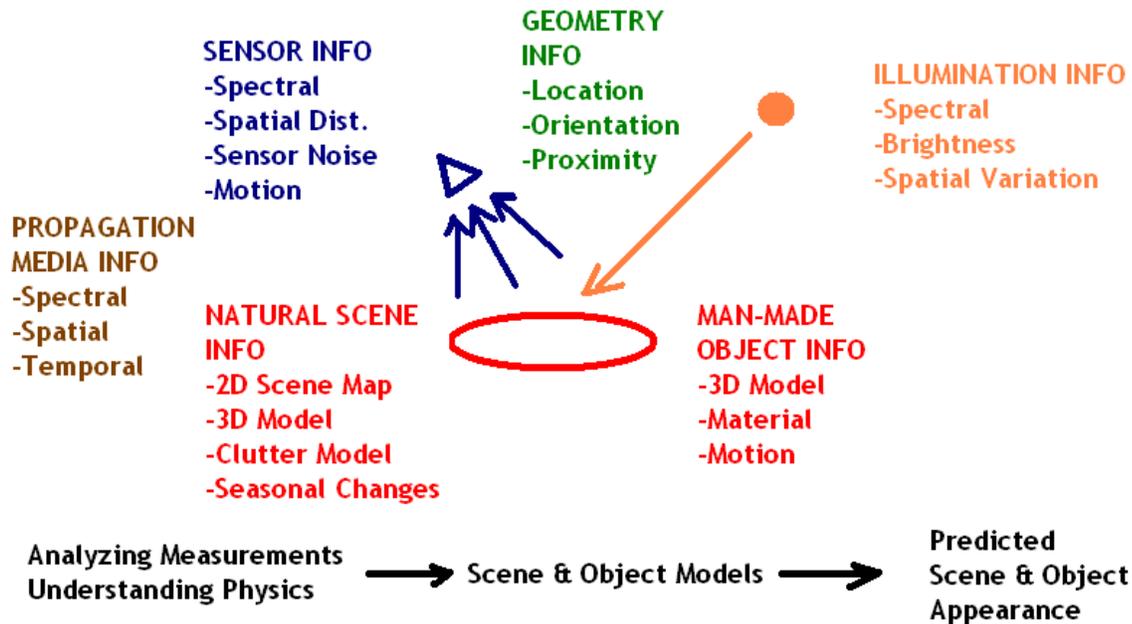
Figure 2: BTF modeling components.

The previous work about BTF modeling can be described by publications that address the BTF model from (a) an image understanding view using textons [7], tree grammars [8] or material models [13], (b) a geometrical optics view using physics laws and surface facet models [5], [6] and (c) a statistical process view using Markov random field [9], joint statistics [10] or filters [14].

The major advantages of our BTF modeling approach over other approaches are (a) the low computational requirements (fast BTF model building, small BTF model storage, fast BTF model-based generation), (b) flexibility of the Johnson family of PDFs to cover a wide range of PDF shapes and (c) applicability of the BTF model to a wide range of spectral sensors, e.g., color, multi-spectral or hyperspectral cameras. Our approach can easily re-use historical data, for example, CURet Database (see http://www1.cs.columbia.edu/CAVE/curet/) or Brodatz & VisTex databases (see http://www-white.media.mit.edu/vismod/imagery/VisionTexture/vistex.html), similar to the re-use of Ulaby measurements [12] in the case of synthetic aperture radar (SAR) sensors for modeling with Weibull PDF model [2]. In addition, the proposed statistical BTF model can interpolate parameters between measurements and thus (a) decrease memory requirements for storing BTF measurements at finer angular increments, and (b) generate BTF predictions for previously unseen viewpoints.

The paper is organized as follows. Section 2 presents a theoretical analysis of modeling approaches to motivate our chosen statistical intensity based approach over facet geometry based approach. In Section 3, we outline a novel system for acquiring data for BTF modeling. Section 4 describes our proposed statistical intensity based model using Johnson family of PDFs. Section 5 presents several issues related to building a database of BTF parameters followed by experimental results summarized in Section 5.3. Our overview remarks and future directions conclude the paper in Section 7.

2. RELATING SENSOR RESOLUTION TO THE ELEMENTS FORMING MATERIAL SURFACE

The color of an object depends on the reflection of light from the object to the eye. Let us assume that an object surface dA is measured by one sensor (pixel) value and the impinging light wavelength lambda on the object surface is much smaller than dA. If an object surface is flat and color homogeneous then the Snell's laws of reflection and refraction can be applied. However, the Snell's laws cannot be directly applied for most surfaces that are not perfectly smooth. For the

case of rough surfaces, researchers have modeled surfaces as a set of small facets, each of which reflects the light according to Snell's laws [5]. This type of modeling will be sufficiently accurate only for surfaces that can be approximated with sufficiently large number of facets under the geometrical optics constraint relating a facet size, wavelength lambda and object surface dA measured by one pixel, such as, lambda << facet size << dA. The concept of modeling accuracy is illustrated in Figure 3. According to Figure 3, we can no longer create enough facets to guarantee surface model accuracy for objects that do not satisfy the right side of the above inequality. Thus, modeling based on facet approximation of object geometry might be less accurate than modeling based on statistical intensity approximation of object appearance.
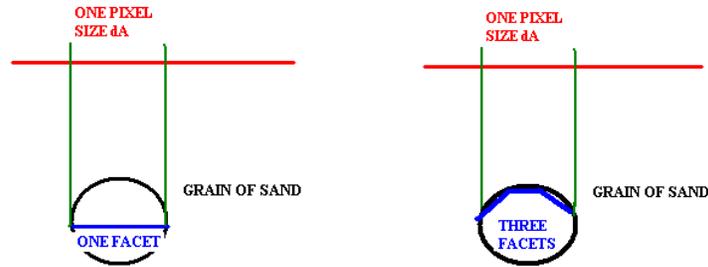

Figure 3: Facet modeling of surface roughness. Spherical surface approximation with one (left) or three (right) facets will determine the accuracy of the surface model.

To illustrate the problem of modeling approach selection, we chose sand grains as a common outdoor clutter type and derived the rule for choosing either "facet approximation" based models or "statistical intensity approximation" based models. We assume that the incident light is in the visible spectrum; wavelength lambda is between 400nm (blue) and 700nm (red). The sand grains are modeled geometrically as spheres with a diameter between 0.02 and 2mm according to the measurements conducted by other scientists in [1]. We related variables from the geometrical optics constraint that formed the worst-case scenario, such as, the smallest grain of sand (diameter=0.02 mm) and the largest wavelength (lambda = 700nm).

The inequality lambda << facet size << dA is assumed to be satisfied if the larger variable is at least n times larger than the smaller variable. Specifically, facet size is 1000 times smaller than the pixel size dA so that, for instance, a sphere can be accurately modeled with at least 1000 micro-facets. Furthermore, a square micro-facet is at least 1000 times larger than wavelength lambda squared and it can accommodate at least 100 rays of lambda size. Thus, the inequalities can be written as $1,000*1,000*100*(lambda)^2 < 1,000*facet$ size $< dA$ with dA (square pixel area) equal to the viewing area of one sand grain; dA = $(0.02mm)^2 = 4x10^8$ [nm^2]. Taking one of the values from dA, diameter and lambda (red) as a constant imposes upper or lower bounds on the other variables as it is illustrated next.
(1) The value of dA imposes upper bounds on diameter and lambda, such as,
Facet size $< 4x10^5$ [nm^2] => diameter $< 2*Sqrt(4x10^5/(4*PI))$ [nm] = 356.82 [nm].
Lambda $< Sqrt(4x10^8/10^8)$ [nm] = 2 [nm].
(2) The value of lambda=700 nm imposes a lower bound on diameter:
$10^8*(lambda=700nm)^2 = 49x10^{12}$ [nm^2] $< 1000*4*PI*(r)^2$
diameter $> 2*Sqrt(49x10^9/(4*PI)) = 124,888.688$ [nm] = 0.125 [mm]
(3) The value of diameter=0.02mm imposes an upper bound on lambda:
$10^8*(lambda)^2$ [nm^2] $< 1000*4*PI*(0.02mm/2)^2 = 1.26x10^{12}$ [nm^2]
lambda $< Sqrt(1.26x10^4) = 112.1$ [nm]

In a summary, all derived upper or lower bounds suggest choosing the "statistical intensity approximation" based models for sand clutter modeling rather than "facet approximation" based models. Under the geometrical optics constraint, the permissible values of one of the independent variables in each case would not satisfy the derived bounds and "facet approximation" based models would lead to very inaccurate predictions. Although this study did not compare qualitatively multiple model approaches, it illustrated the need for alternative approaches for BTF modeling at fine scale for objects of the sand grain size.

3. ROBOTIC SYSTEM FOR LABORATORY BTF DATA ACQUISITION

We have developed a prototype robotic system for BTF data acquisition that could be used potentially outdoor and in hazardous indoor environments. We envision such a system to be used in an autonomous mode or in a remotely controlled mode for BTF data acquisition. The acquired data can be used in two ways. First, the BTF data can be sent wirelessly to a central base station and used for prediction of scene clutter observations in order to improve the robustness and accuracy of ATR. Second, the BTF data can be processed onboard of the robot and used for ATR directly by the robot. Based on our preliminary work, we have not encountered enormous computational requirements for the onboard BTF model formation.

In our laboratory setup, we used a wireless (2.4GHz), color, light-weighted, stealth camera that was attached to a griper of the robotic arm. The robotic arm is mounted on a robot made by ActivMedia Robotics (see http://www.amigobot.com/). The viewing angles were programmed to be ten degrees apart. Our prototype system was tested with matchbox cars (ATR applications) and several samples of sand in a plate (scene clutter modeling application) as it is illustrated in Figure 4. In comparison with other setups where the object/sample is being rotated while the camera is fixed (e.g., the setup for building the CURet database), our BTF data acquisition setup can obtain BTF measurements from viscous materials, for example, sand, which is not possible with many other systems.

Figure 4: Robotic system for BTF data acquisition. Object BTF modeling (left) for ATR applications and clutter BTF modeling (right) for scene understanding and simulation applications.

4. BTF MODEL USING JOHNSON PDF FAMILY

In order to build BTF models, we need to estimate (1) what PDF model matches the measured samples best, and (2) what parameters of the selected PDF fit the data best. Data histograms as PDF approximations of measurements can take many different shapes. It is known that a single PDF model is usually not flexible enough to accurately model all occurring histogram shapes. One approach to this problem is to use a set of distributions, for instance, Normal, Weibull, Exponential, Rayleigh, Lognormal, etc, under the assumption that one would know how to select the most appropriate PDF model. Another approach is to use a family of PDFs that can model multiple shapes.

In this work, we chose a family of PDFs proposed by Johnson [11]. The Johnson family consists of three families of distributions S_L, S_B and S_U that are generated by three transformations $\tau_i(x, \varepsilon, \lambda); i = 1, 2, 3$ showed in Equation 1.

$$z = \gamma + \eta\tau(x;\varepsilon,\lambda);\, \eta > 0;\, -\infty < \gamma < \infty;\, \lambda > 0;\, -\infty < \varepsilon < \infty$$

$$S_L : \tau_1(x;\varepsilon,\lambda) = \ln(\frac{x-\varepsilon}{\lambda});\, x \geq \varepsilon$$

$$S_B : \tau_2(x;\varepsilon,\lambda) = \ln(\frac{x-\varepsilon}{\lambda+\varepsilon-x});\, \varepsilon \leq x \leq \varepsilon + \lambda$$

$$S_U : \tau_3(x;\varepsilon,\lambda) = \sinh^{-1}(\frac{x-\varepsilon}{\lambda});\, -\infty < x < \infty$$

(Eq. 1)

The resulting random variable z follows the standard normal distribution and is obtained by using the first expression in Equation 1. These three transformations lead to a family of three PDFs described in Equation 2 and characterized by four parameters $\gamma, \eta, \varepsilon$ and λ.

Johnson S_B

$$f_2(x) = \frac{\eta}{\sqrt{2\pi}} \frac{\lambda}{(x-\varepsilon)(\lambda-x+\varepsilon)} \exp\left\{-\frac{1}{2}\left[\gamma + \eta\ln(\frac{x-\varepsilon}{\lambda-x+\varepsilon})\right]^2\right\};$$

$$\varepsilon \leq x \leq \varepsilon + \lambda, \eta > 0, -\infty < \gamma < \infty, \lambda > 0, -\infty < \varepsilon < \infty$$

Johnson S_L

$$f_1(x) = \frac{\eta}{\sqrt{2\pi}(x-\varepsilon)} \exp\left\{-\frac{1}{2}\left[\gamma + \eta\ln(\frac{x-\varepsilon}{\lambda})\right]^2\right\};$$

$$x \geq \varepsilon, \eta > 0, -\infty < \gamma < \infty, \lambda > 0, -\infty < \varepsilon < \infty$$

(Eq. 2)

Johnson S_U

$$f_3(x) = \frac{\eta}{\sqrt{2\pi}} \frac{1}{\sqrt{(x-\varepsilon)^2 + \lambda^2}} \exp\left\{-\frac{1}{2}\left[\gamma + \eta\ln\left((\frac{x-\varepsilon}{\lambda}) + \left[(\frac{x-\varepsilon}{\lambda})^2 + 1\right]^{1/2}\right)\right]^2\right\};$$

$$-\infty \leq x \leq \infty, \eta > 0, -\infty < \gamma < \infty, \lambda > 0, -\infty < \varepsilon < \infty$$

The process of fitting the Johnson family to measured data consists of two steps; selecting one of the three PDF models and estimating its parameters. The selection step is achieved by calculating the standard central moments from the measured data (β_1 and β_2) and choosing the PDF model based on the statistical probability plane shown in Figure 5. The parameters for a selected PDF model are found using a lookup table for the function according to [11]. Slipfker and Shapiro [11] describe a method that allows us to quickly estimate parameters based on four well-chosen sample points in the dataset.
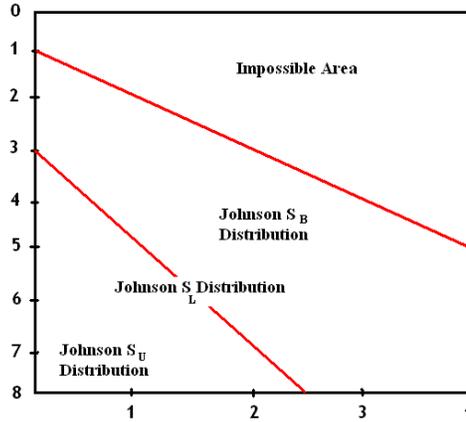
Figure 5: Selection of one of the Johnson PDF. (β_1 – horizontal axis and β_2 - vertical axis).

Once all parameters are estimated for a chosen PDF model we use Equation 1 to generate BTF predictions. We estimate *x* given in Equation 2 by generating random numbers following a standard normal distribution and transforming them accordingly since the random variable *z* follows normal distribution.

Figure 6 shows some of the diverse PDF shapes that the particular Johnson S_B distribution can model. If we had chosen the modeling approach using multiple distribution models, then we would have needed to use an exponential, Beta, Gaussian and Uniform PDF models to approximate the same set of PDF shapes.
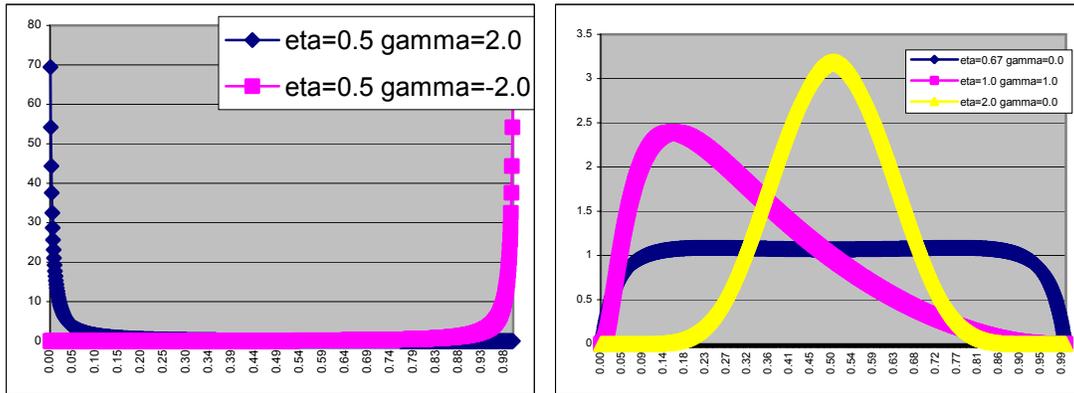

Figure 6: Examples of PDF shapes that the Johnson Sb PDF can model by varying eta and gamma parameters (lambda = 1, epsilon =0).

5. BUILDING A DATABASE OF PDF PARAMETERS

The task of building a database of PDF parameters requires to address the issues of (a) image feature selection (color space selection), (b) clutter segmentation (or mask generation) and (c) BTF statistical quality metric definition. We omitted the issue of database storage and information retrieval in this paper.

5.1. Optimal Feature Space For Statistical BTF Modeling
Given a set of measurements acquired at multiple view angles, we investigated several features that could be represented with our proposed statistical BTF model. This issue of feature selection is related to the fact that multi-band (multi-

wavelength) measurements are usually characterized by large cross band correlation and hence statistical model of each band separately would ignore the conditional dependencies across multiple bands. For the case of red, green and blue (RGB) measurements, there are already existing other color spaces than RGB, for example, hue, saturation and value (HSV) space, which decompose the color into perceptually independent features. In our current work we focused on evaluating both RGB and HSV feature spaces. We plan to address this issue by other techniques for multi-spectral or hyperspectral measurements in future.

5.2. Mask Creation

After acquiring all images, there is a need to remove background and partition each image into regions corresponding to appropriate clutter types. We have used three different approaches to image partitioning, such as, (1) image clustering using advanced K-means method (called Isodata algorithm and implemented in [4]), (2) bottom-up image segmentation algorithm using similarity analysis [3] and (3) manual image partitioning using MS Paint. These three approaches resulting in a mask that contain unique labels per each clutter type with either spatially contiguous or non-contiguous labeled regions. We present results for all three types of masks.

5.3. BTF Statistical Quality Metrics (Verification And Validation)

It is critical for any new modeling approach to obtain quantitative measures of the prediction fidelity. The verification and validation of the proposed BTF model requires defining quality metric. We investigated several metrics and decided to use correlation coefficient and normalized histogram metrics. The correlation coefficient metric is defined in Equation 3. The development of other statistical quality metrics is currently in progress.

$$r = \frac{\sum_i (x_i - x_{avg})(y_i - y_{avg})}{\sqrt{\sum_i (x_i - x_{avg})^2} \sqrt{\sum_i (y_i - y_{avg})^2}}$$

(Eq. 3)

The normalized histogram metric takes two images and a mask and generates a histogram of the combination mask and band of the image. Next it will take the histograms and normalize each of them such that we are left with the percentage of pixels in that band/mask combination that has that intensity. Next we compare the histogram of original image with the histogram of the test image subtracting each bin of the histogram and adding the difference. The value calculated this way is the total difference for the band/mask combination. The total error per mask is the total of the bands.

Besides these two methods to compare images, many more exist and will give us a better understanding of how well our method performs. We are planning on adding X^2 as well as simple image comparison in the future. At the same time we will add methods to do these test with images that have had a PCA applied, this should give us a better measurement across bands.

6. EXPERIMENTAL RESULTS

We performed two experiments with laboratory data and aerial photography data. The analysis of the experimental data was conducted according to our proposed statistical BTF modeling approach by processing image features in RGB and HSV color spaces. In the first experiment we used a robot, a robotic arm with a wireless camera held by the gripper of the robotic arm, a stationary pan-tilt-zoom Sony camera and an orientation tracker mounted on the Sony camera to accurately measure its viewing position. We acquired test data of multiple objects and clutter types at certain angles and generated synthetic unseen images. In the second experiment we processed an aerial image by partitioning the image, extracting BTF model parameters and recreating the original image based on the BTF model.

6.1. Laboratory Data

We conducted an experiment with black and white sand in order to validate that we can accurately generate unseen images of black and white sand based on our BTF model. First, we extracted statistical BTF model for a plate of black sand (see Figure 7) and a plate of white sand. We used both a robot equipped with a camera as well as a stationary camera to take snapshots of the plates of sand. In order to delineate the background from the sand regions, we manually created a mask. All BTF parameters for different viewing angles and two clutter types were stored in a database.

Figure 7: Sand clutter data for 90, 70, 50 and 30 degrees view angles (left to right).

After forming the database of PDF parameters, we created a test plate with half white and half black sand, separated in the middle as shown in Figure 8 (left). We used our camera setup to take pictures of this test plate at the same angles as the other single color sand plates. The mask for a mixed color sand plate was formed and used for generating a synthetic unseen image based on the BTF model stored in a database. A comparison of the synthetic image and the measured mixed color sand image resulted in a correlation coefficient equal to 0.97 (see Figure 8).
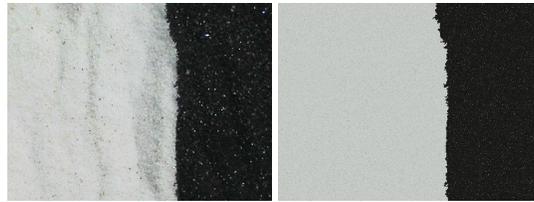

Figure 8: Measured image (left) and synthetic unseen image (right).

6.2. Aerial Photography Data

In the second experiment we primarily evaluated multiple image partitioning methods for clutter masking. The test image was an aerial photograph of a farmland in central Illinois. We used automated clustering (no constraint on labels to form a contiguous regions) and segmentation (spatially constrained to form contiguous regions) algorithms as well as manual methods to create masks of the aerial image, where each color of the mask corresponded to a unique clutter region. We used these masks to extract the BTF models from the aerial images. Next, we re-generated a synthetic image of the original image based on built BTF model and the masks created earlier. Figure 9 illustrates a perceptual comparison of measured and re-generated images.

Figure 9: Color (RGB) aerial photograph (left) and its simulation based on the proposed BTF model (right).

6.3. Experimental Evaluations

Given the data sets described in previous sections, we aimed at demonstrating (a) the concept of the proposed statistical BTF modeling approach and (b) the uncertainty introduced by data pre-processing (e.g., methods for clutter masking) and feature selection (e.g, RGB or HSV color spaces). We provide results in Table 1 for multiple masks and two color spaces using the correlation coefficient metric defined in Equation 3. The correlation coefficient is computed over a mask shown in Figure 10 (left). In order to demonstrate the correlation coefficient changes in magnitude, one of the baseline images is the original image (correlation equal to 1) with inserted red lines Figure 10 (right) that lead to RGB correlations equal to [0.97, 0.92, 0.99]. All results from Table 1 are graphically visualized in Figure 11.
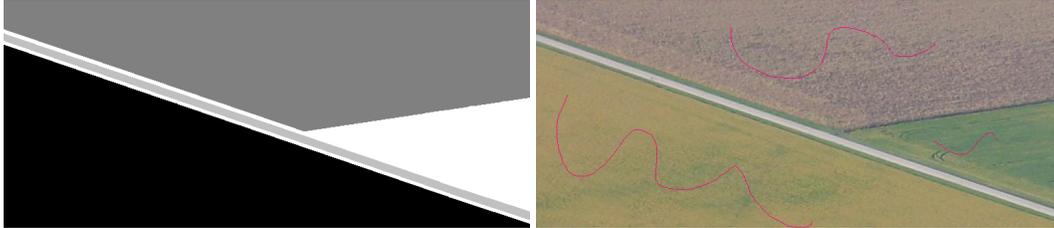

Figure 10: Manually obtained clutter mask (left). Color (RGB) aerial photograph with inserted red lines for testing the correlation metric (right).

Table 1: Correlation coefficients computed from the original aerial photograph and generated synthetic images using multiple masking methods. Perfect – original image, scratch – image with inserted red lines, paint – manually created mask, rgb – RGB color space, hsv - HSV color space, iso5 – the mask created by using Isodata clustering algorithm with 5 labels (clusters), iso8 - the mask created by using Isodata clustering algorithm with 8 labels, isopaint - the mask created by using Isodata clustering algorithm and manually adjusted to form contiguous regions.

Mask&Features\Band	Red	Green	Blue
Perfect & rgb	1	1	1
Scratch & rgb	0.972013	0.918532	0.988359
paint & rgb	0.636607	0.588386	0.834411
paint & hsv	0.661613	0.554613	0.833382
iso5 & rgb	0.713721	0.732382	0.817106
iso5 & hsv	0.73289	0.649264	0.827051
iso8 & rgb	0.71428	0.434226	0.728956
isopaint & rgb	0.68279	0.636866	0.847646

Furthermore, to compare the performance of the Johnson family PDFs and other statistical PDF models, we have taken images of black sand, white sand and the test image with both types of sand. We created masks for each of these images and estimated parameters of the black sand, and the white sand regions using multiple PDF models. We used then selected PDF models, their estimated PDF parameters and the mask corresponding to the test image with both clutter types, to generate a new image. Ideally, the generated image should be identical with the measured test image. We compared the test and generated images based on normalized image histograms. Table 2 lists the comparison results obtained by using different statistical PDF models for black and white sand (mask labels 0 and 15). As it can be seen from the total error (sum of all column errors), the Johnson family PDF models generate the most similar image to the test image according to this metric. Table 2 also shows that the Johnson family outperforms other PDF models in terms of the normalized histogram error for almost all rows (or all combinations of mask label and band).
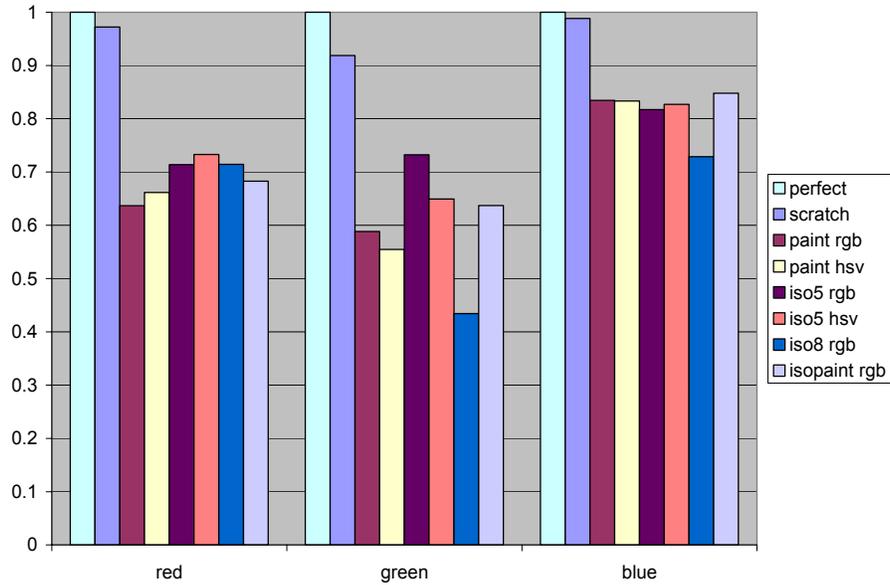
Figure 11: Visualization of the correlation coefficients from Table 1.

Table 2: Difference in normalized histograms.

Mask Label	Band	Johnson	Gaussian	Uniform	Weibull
0	0	0.2814	0.5628	1.9084	0.8435
0	1	0.3648	0.5892	1.9009	0.6475
0	2	0.3857	0.5675	1.8994	0.8854
15	0	0.4701	0.4789	1.9293	0.4277
15	1	0.4759	0.4888	1.9102	0.4947
15	2	0.4443	0.4543	1.9279	0.3401
Total Error		2.4225	3.1418	11.4762	3.6392

Not only are we looking for an accurate statistical model to use, but also we are focusing on a fast prediction model. We believe that generating a 1,000x1,000 image in less than a couple of seconds is sufficiently fast considering java implementation and a desktop personal computer. Table 3 shows the times it takes to generate one million random samples using different PDF models. As it can be seen generating samples using the uniform PDF model is the fastest prediction model followed by Gaussian and Johnson. However, all three methods are capable of generating one million samples in less than a second.

Table 3: Time to generate one million random samples.

PDF	Time
Johnson	937 ms
Gaussian	641 ms
Uniform	406 ms
Weibull	2187 ms

7. SUMMARY

We have presented a novel approach to multi-sensor statistical modeling of bi-directional texture functions. Our work on BTF modeling has focused on (1) relating a sensor resolution to the size and shape of elements forming material surface with the goal of identifying criteria for choosing statistical intensity based approach over facet geometry based approach, (2) developing a robotic system for laboratory BTF data acquisition with the goal of autonomous BTF data acquisition for multiple applications, (3) extracting and generating the PDF parameters of the Johnson family as the primary BTF model representation, (4) selecting optimal feature space with the goal of de-correlating bands, (5) building a database of parameters for the Johnson family of PDFs for two sand clutter types to prove the BTF modeling concept and (6) researching several statistical quality metrics that can be used for verification and validation of the obtained BTF models. We have recorded computational times for building and generating BTF models of sand clutter types and the times are negligible with any other approach that we are aware of.

REFERENCE:

[1] *Glossary. Erosion and Sediment Control Management System. Lake Macquarie, Australia: 9 September 1999.*

[2] Bajcsy, P., D. Sullivan, and P. Ryan. *Estimating Weibull Distribution Parameters*. in *Intelligent Engineering Systems Through Artificial Neural Networks*. 2000: ASME Press, New York.

[3] Bajcsy P., and N. Ahuja, "Hierarchical Clustering of Points Using Similarity Analysis" IEEE Transactions on Pattern Analysis and Machine Intelligence, VOL. 20, NO. 9, pp. 1011-1015, September 1998.

[4] Bajcsy, P. et. al., Image To Knowledge (I2K)," Software Overview and Documentation, ALG NCSA, UIUC, IL, URL: http://alg.ncsa.uiuc.edu/tools/docs/i2k/manual/index.html.

[5] Dana, K.J., et al., *Reflectance and texture of real-world surfaces.* ACM Transactions on Graphics, 1999. 18(1): p. 1-34.

[6] Dana, K.J. and S.K. Nayar. *Correlation Model for 3D Texture*. in *International Conference Computer Vision*. 1999.

[7] Leung, T.K. and J. Malik. *Recognizing Surfaces using Three-Dimensional Textons*. in *International Conference Computer Vision*. 1999.

[8] Lu, S.Y. and K.S. Fu, *Stochastic Tree Grammar Inference for Texture Synthesis and Discrimination.* Computer Graphics and Image Processing, 1979. 9: p. 234-245.

[9] Panjwani, D.K. and G. Healey, *Markov Random Field Models for Unsupervised Segmentation of Textured Color Images.* IEEE Transactions on Pattern Analysis and Machine Intelligence, 1995. 17(10): p. 939-954.

[10] Portilla, J. and E.P. Simoncelli, *A Parametric Texture Model Based on Joint Statistics of Complex Wavelet Coefficients.* International Journal of Computer Vision, 2000. 40(1): p. 49-70.

[11] Slipfker, J.F. and S.S. Shapiro, *The Johnson System: Selection and Parameter Estimation.* Technometric, 1980. 22(2): p. 239-246.

[12] Ulaby, F.T. and M.C. Dobson, *Handbook of Radar Scattering Statistics for Terrain*. 1989, Norwood, MA: Artech House.

[13] Varma, M. and A. Zisserman. *Classifying Images of Materials: Achieving Viewpoint and Illumination Independence*. in *European Conference on Computer Vision*. 2002.

[14] Zhu, S.C., Y. Wu, and D. Mumford, *Filters random fields and maximum entropy (FRAME): To a unified theory for texture modeling.* International Journal of Computer Vision, 1998. 27(2): p. 1-20.